Influence of substrate-mediated interactions on the self-organization of adatom clusters

Qiyang Hu* and Nasr M. Ghoniem†
Mechanical and Aerospace Engineering Department, University of California, Los Angeles, California 90095-1597, USA

Daniel Walgraef
Center of Nonlinear Phenomena and Complex Systems, Free University of Brussels, CP 231, Boulevard du Triomphe, B-1050 Brussels, Belgium

(Received 4 April 2006; revised manuscript received 25 October 2006; published 5 February 2007)

We investigate here the evolution of self-organized monolayer atomic clusters on atomically flat substrates during epitaxial deposition. A phase field-model is developed for the free energy of the system, which includes short-range as well as long-range interactions between deposited atom clusters mediated by the substrate, using the elastic theory of intrinsic surface stress. Natural self-organization of surface atomic clusters is shown to result from reaction-diffusion kinetics, where patterns are either dots or stripes, at low (high) and intermediate coverage, respectively. Cluster-cluster interactions slightly favor stripes. The length scale of natural self-organized structures is in the tens of nanometers range. Imposition of a substrate periodic strain field by subsurface interfacial dislocations is shown to dramatically change the self-organized pattern and its length scale. Qualitative agreements between model predictions and experimental observations on self-organized Ge quantum dots on Si substrate are demonstrated.

DOI: 10.1103/PhysRevB.75.075405 PACS number(s): 68.43.Hn, 68.43.De, 68.47.Fg, 81.40.Jj

I. INTRODUCTION

An important direction in nanoscience research is the potential utilization of self-organization phenomena in epitaxial thin-film growth to manufacture ultrasmall structures for future electronic and photonic devices. However, realistic advances in this technology much depend on providing the means for atoms to assemble themselves in a precise manner and to control their size distribution during the fabrication process. For example the fabrication of massive numbers of well-aligned quantum dots on two-dimensional (2D) substrates or in 3D stacks is clearly challenging and requires both theoretical and experimental advances.

In most cases, the length scale of the system characterized by the applied external field is on the order of microns. However, self-organized patterns are usually much finer, with a length scale on the order of tens of nanometers. Thus coupling between these scales becomes a *multiscale* modeling problem. Atomistic simulations can only provide information on some of the physical mechanisms. Specifically, in molecular dynamics (MD) simulations, the required deposition rate needs to be unrealistically high, while the computational time in Monte Carlo (MC) methods to simulate thin-film growth under realistic deposition rates is still excessive.[1,2] A more serious physical problem is that self-organization effects during thin-film deposition can hardly be explained only by the behavior of single adatoms. Investigations[3,4] have already shown that collective effects of atomic clusters play a more decisive role in film processes, especially in the presence of a very weak elastic field in the substrate. Hence continuum approaches which intrinsically consider the film as a continuous distribution of atomic surface density exhibit an advantage, especially for simulation of the self-ordering behavior in larger dimensions and for longer time scales than can be obtained with atomistic simulations.

The basic idea of continuum modeling is to represent the film surface by a set of meshed mesoscopic cells. Atom fluxes can exist between neighboring cells. Because of its mesoscopic scale, all spatial fluctuations within each cell, such as texture and microstructures, are ignored and the mean-field approach is a reasonable approximation. Mathematically, the model is expressed in terms of reaction-diffusion equations of the 2D Cahn-Hilliard partial differential equation type. Thus, the self-organization pattern is understood as an underlying instability that results from the interplay between local interfacial interactions of cell boundaries and global substrate-mediated interactions. This approach has been used in studying structural transformations in 2D and 3D solids,[5–7] and phase separations on surfaces.[8–10] By taking different phases as occupied adatoms and vacancy sites, Walgraef developed a dynamic model of the reaction-diffusion type, where the self-organized pattern is described as a result of the evolution of the mean surface adatom coverage.[11] The advantage of this model is that it includes the effects of many relevant experimental parameters, such as deposition rates, substrate temperature, and atomic mobility.

However, Walgraef's original model does not explicitly include interactions between atomic clusters and substrates, and hence allows for studies of "natural" self-organization only. If the deposition amount of atoms is very high such that atomic clusters become 3D islands, thin films can be considered as bulk solids. Thus the evolution of multilayer clusters (islands) can be described as a surface roughening problem having Asaro-Tiller-Grinfeld (ATG) instability, in which both bulk and surface elastic energy play a role.[12,13] However, for monolayer structures, surface stresses interplay with interfacial energies prescribed by nearest-neighbor (NN) interactions to determine the evolving pattern nature.[14] Due to the existence of capillary effects, a monolayer atomic cluster can be regarded as a defect with a force dipole density distributed along the surface.[15,16] The interaction between two monolayer (ML) clusters can thus be represented by the interaction between two force dipole densities mediated by the substrate.

This idea has been adopted by Suo and Lu and elasticity effects are included by a classical Cerruti solution in which the elastic field in the half space is due to a tangential point force acting on the surface.[8,9]

In the present paper, we present a phase-field model for self-organized monolayer atomic clusters extending the original model of Walgraef to include substrate-mediated interactions. The present work also builds on the approach of Suo and Lu,[8,9] where we consider the additional effects of kinetic absorption and desorption rates as well as weak external fields. We include here adsorption and desorption processes so that pattern selection is of a dynamic nature and can thus be dependent on the kinetic rates of deposition and evaporation. In addition, we distinguish the effects of externally applied elastic fields from intrinsic long-range fields generated by cluster-cluster interactions. It will be shown here that a nonuniform ultra weak external strain field can dramatically change the self-organized pattern and its length scale. Such external fields can be used as templates for "directed" self-organization of surface clusters. A periodic external strain field can be realized in the substrate, generated by, for example, interfacial dislocation networks,[17,18] buried quantum dots,[19] or void lattices.[20]

In Sec. II, a formulation that includes long-range (LR) substrate-mediated interactions and the presence of a nonuniform periodic external elastic field is developed. The numerical method to solve the governing equation is described in Sec. III. In Sec. IV, we discuss the nature of an external field generated from a buried interfacial dislocation network in Si-Ge heterepitaxial strutures, and we show a qualitative agreement between model predictions and experimental observations. In Sec. IV, LR effects in crystals with cubic elastic symmetry (e.g., SiGe) are studied within the framework of a linear stability analysis.

II. FORMULATION

A continuous model for the surface adatom concentration can be constructed within the framework of chemical kinetics via the following mass conservation equation:

$$\frac{\partial c}{\partial t} = \alpha(1-c) - \beta c - \nabla \cdot \mathcal{J}, \tag{1}$$

where $c(\mathbf{r},t)$ is the concentration of adatoms on the substrate. The reaction process is represented by the adsorption and desorption rates (α and β). The diffusion flux $\mathcal{J}$ is determined by linear nonequilibrium thermodynamics. It should be noted that Eq. (1) is a deterministic equation of motion for the phase-field variable c. Based on the field-theoretic model by Langer[21] the *et al.*[22] the nucleation process has been included by the above mesoscopic atomic dynamics. In the present paper, we will ignore the stochastic thermal fluctuations, because the deterministic and stochastic models produce patterns which are qualitatively similar to the microstructures observed during spinodal decomposition.[23,24] With Onsager's assumptions for an isothermal process and the fact that the chemical potential is the functional derivative of the free energy, we have the following expression for the atomic mass flux $\mathcal{J}$ for a single specie adsorbate layer.[25]

$$\mathbf{J} = -L\nabla\mu_c = -L\nabla\frac{\delta\mathcal{F}}{\delta c}, \tag{2}$$

where L is the atomic mobility ($L=D/k_BT$) and D is the surface diffusion coefficient. $\mathcal{F}$ is the free energy of adsorbed atoms. Thus, we need to obtain an explicit expression for the free energy functional $\mathcal{F}$. Here we consider $\mathcal{F}$ to consist of three parts as

$$\mathcal{F} = \mathcal{F}^{(a)} + \mathcal{F}^{(s)} + \mathcal{F}^{(c)}, \tag{3}$$

where $\mathcal{F}^{(a)}$ denotes direct interaction (nearest neighbor) between adatoms, $\mathcal{F}^{(s)}$ for their interaction with the substrate, and $\mathcal{F}^{(c)}$ for the indirect (through substrate and long-range) interaction between clusters of atoms.

To determine $\mathcal{F}^{(a)}$, we begin by writing the Hamiltonian of a discrete lattice system of adparticles on the substrate between which two-body interactions exist:

$$\mathcal{H}^{(a)} = \frac{1}{2}\sum_{ij}\epsilon_{ij}^{(a)}s_is_j, \tag{4}$$

where s_i is the occupation number at site i, which takes a value of 0 or 1. The two-body interaction energy $\epsilon_{ij}^{(a)}$ is taken negative for attractive interactions. Due to the difficulty in having a precise evaluation of the partition function for this Hamiltonian, we first approximate it by the mean-field Hamiltonian

$$\mathcal{H}_0 = k_BT\sum_i \lambda_i s_i, \tag{5}$$

where $k_BT\lambda_i$ denotes the mean interaction energy of an adatom at site i. The corresponding mean-field partition function is

$$\mathcal{Z}_0 = \prod_i \sum_{s_i=0,1} \exp(-\lambda_i s_i) = \prod_i \frac{1}{1-c_i}, \tag{6}$$

where $c_i=1/(1+\exp\lambda_i)=\langle s_i\rangle 0$, which is the equilibrium average of the mean-field occupancy number at site i. This is a continuous variable varying between 0 and 1, which is just the coverage of adsorbed particles. The mean-field free energy is

$$\mathcal{F}_0 = -k_BT\ln\mathcal{Z}_0 = k_BT\sum_i \ln(1-c_i). \tag{7}$$

By the variational mean-field theory, the free energy can be approximated as

$$\mathcal{F}^{(a)} \approx \mathcal{F}_0 + \langle\mathcal{H}^{(a)} - \mathcal{H}_0\rangle_0. \tag{8}$$

From Eq. (4) and (5), we have

$$\langle\mathcal{H}^{(a)} - \mathcal{H}_0\rangle_0 = \frac{1}{2}\sum_{ij}\epsilon_{ij}^{(a)}c_ic_j - k_BT\sum_i\lambda_ic_i. \tag{9}$$

Thus, the free energy in Eq. (8) takes the form

$$\mathcal{F}^{(a)} = k_BT\sum_i[(1-c_i)\ln(1-c_i) + c_i\ln c_i] + \frac{1}{2}\sum_{ij}\epsilon_{ij}^{(a)}c_ic_j. \tag{10}$$

The last expression can also be obtained from thermodynamic considerations alone by noting that the first sum is due to mixing entropy and the second represents the interaction enthalpy. A continuum expression can be obtained by taking the continuous limit of the above discrete equation [$\Sigma_i \rightarrow \int d\mathbf{r}$ and $c_i \rightarrow c(\mathbf{r})$], in which we pass from an average over a collection of lattice sites to an average of coarse-grained cells with mesoscopic scales. Especially for the last term in Eq. (10), assuming there is only nearest-neighbor interactions, which means $\epsilon^{(a)}(\mathbf{r},\mathbf{r}') \approx -\gamma\epsilon\delta(|\mathbf{r}-\mathbf{r}'|=a)$, where γ is the lattice coordination number, ϵ is the pair interaction energy, and a is the lattice constant, we could obtain the interfacial terms using the fact that $2c(\mathbf{r})c(\mathbf{r}')=c^2(\mathbf{r})+c^2(\mathbf{r}')-[c(\mathbf{r})-c(\mathbf{r}')]^2$. With similar arguments proposed by Walgraef,[11] we have

$$\int_S d\mathbf{r}'\,\epsilon^{(a)}(\mathbf{r},\mathbf{r}')c(\mathbf{r})c(\mathbf{r}') = -\epsilon_0 c^2(\mathbf{r}) + \xi_0^2|\nabla c(\mathbf{r})|^2, \quad (11)$$

in which $\epsilon_0=-\Sigma_j\epsilon_{ij}=\gamma\epsilon$, $\xi_0^2=a^2\gamma\epsilon$, and the integral is taken over the surface. The first term represents energy reduction due to NN local interactions, while the second accounts for the extra interfacial energy associated with clustering gradients.

Thus, Eq. (10) becomes

$$\mathcal{F}^{(a)} = \int_S d\mathbf{r}\left[k_B T f(\mathbf{r}) - \frac{1}{2}\epsilon_0 c^2(\mathbf{r}) + \frac{1}{2}\xi_0^2|\nabla c(\mathbf{r})|^2\right], \quad (12)$$

where $f(\mathbf{r})=[1-c(\mathbf{r})]\ln[1-c(\mathbf{r})]+c(\mathbf{r})\ln[c(\mathbf{r})]$. The chemical potential of this NN interaction is

$$\mu^{(a)} = k_B T \ln\left(\frac{c}{1-c}\right) - \epsilon_0 c - \xi_0^2\nabla^2 c. \quad (13)$$

Next, let us consider the calculation of $\mathcal{F}^{(s)}$: the free energy of an adatom interaction with a strained substrate. We treat the variable part of the substrate-mediated free energy by two-body interactions as we did for NN interactions, finally leading to an integral term similar to that in Eq. (11). This treatment is equivalent to considering adatoms as point defects. Although the formulation is successfully adopted in describing structural transformations in solids,[5,7] the situation is different on the surface. Both energy calculations[26] and the Monte Carlo simulations[3] have shown that this point-defect-type interaction on the surface will be so small that it can be completely neglected. An agglomerate effect, which results from many-body interactions, has to be taken account. Here, we adopt a mesoscopic continuum approach as a convenient way to formulate it, in which the discontinuity of intrinsic surface stress between adatom clusters and the substrate provides a large driving force to self-organization behavior.[14,16]

On the edge of a cluster, the geometric discontinuity can be replaced by a pair of tangential force dipoles.[15] The relation between the force density (f_α) and surface intrinsic stress ($\sigma_{\alpha\beta}$) is given by

$$f_\alpha(\mathbf{r}) = \frac{\partial\sigma_{\alpha\beta}(\mathbf{r})}{\partial x_\alpha}, \quad (14)$$

where α and β denotes the indices (1 or 2) on the surface. In our monolayer model, the intrinsic stresses of clusters are treated in an effective manner, as the stress is assumed to be linearly dependent on their concentration and, thus, we have a first-order approximation,[27] expressed by Vegard's law:

$$\sigma_{\alpha\beta}(\mathbf{r}) \approx \sigma_{\alpha\beta}c(\mathbf{r}), \quad (15)$$

where $\sigma_{\alpha\beta}$ is considered a material constant on the homogeneous substrate surface. In the isotropic case, we have

$$\sigma_{\alpha\beta} = \sigma\delta_{\alpha\beta}. \quad (16)$$

The free energy induced by the substrate can be generally expressed as the force times the displacement ($\mathbf{u}$):

$$\mathcal{F}^{(s)} = -\int_S d\mathbf{r} f_\alpha u_\alpha = -\int_S d\mathbf{r}[\sigma\nabla_\alpha c(\mathbf{r})]u_\alpha. \quad (17)$$

Thus, using the interchangable property of derivatives and variational operators and integrating by parts with Gauss's theorem, the chemical potential simply becomes

$$\mu^{(s)}(\mathbf{r}) = \sigma u_{\alpha,\alpha}. \quad (18)$$

Here, if there is a nonuniform displacement field applied to the surface, then the interaction part of the chemical potential ($\mu_e^{(s)}$), which is coverage independent, is

$$\mu_e^{(s)}(\mathbf{r}) = \sigma[\varepsilon_{xx}(\mathbf{r}) + \varepsilon_{yy}(\mathbf{r})], \quad (19)$$

where $\varepsilon_{\alpha\beta}$ is the external strain field applied in the substrate. Since the elastic energy per adatom is approximated as $\sigma_{\alpha\beta}\varepsilon_{\alpha\beta}$, it is easy to see that atomic clusters are considered as parts of the substrate surface that store elastic energy. It should be noted that the term $\mu_e^{(s)}$ is considered only when the field from the substrate is nonuniform. This means that a uniform strain field in a *flat* substrate surface, such as that due to coherent lattice mismatch in heteroepitaxial structures, will not influence self-organized patterns on the surface.

Finally we consider the free energy due to cluster-cluster interactions. This can be expressed in the usual Green's function method with substitution of Eq. (15) into Eq. (14) without any external strain field on the substrate:

$$\mathcal{F}_2^{(s)} = -\frac{1}{2}\int\int d\mathbf{r}d\mathbf{r}' f_i(\mathbf{r})G_{ij}(\mathbf{r}-\mathbf{r}')f_j(\mathbf{r}')$$
$$= -\frac{1}{2}\int\int d\mathbf{r}d\mathbf{r}'\sigma_{ik}\nabla_k c(\mathbf{r})G_{ij}(\mathbf{r}-\mathbf{r}')\sigma_{jl}\nabla_l' c(\mathbf{r}'), \quad (20)$$

where the energy is positive for attractive interactions and we perform a double surface integral in Eq. (20). $G_{\alpha\beta}(\mathbf{r}-\mathbf{r}')$ is the surface Green's function which denotes the displacement component α at position $\mathbf{r}'$ caused by a unit point force acting at position $\mathbf{r}$ in direction β. It is also noted that from symmetry considerations we must have

$$G_{\alpha\beta}(\mathbf{r}-\mathbf{r}') = G_{\alpha\beta}(\mathbf{r}'-\mathbf{r}) = G_{\beta\alpha}(\mathbf{r}-\mathbf{r}').$$

Applying the same techniques used in deriving Eq. (19) and applying the elastic isotropic condition (16), we obtain a coverage-dependent part of the chemical potential ($\mu_c^{(s)}$) as

$$\mu_c^{(s)} = \sigma^2 \int_S d\mathbf{r}'[\nabla_\alpha G_{\alpha\beta}(\mathbf{r}-\mathbf{r}')\nabla'_\beta c(\mathbf{r}')]. \tag{21}$$

Substituting Eqs. (13), (19), and (21) into Eq. (2) and then into Eq. (1), we finally obtain a "phase-field" kinetic equation, given for the continuum concentration c as

$$\partial_t c = \frac{1}{\tau}(c_0 - c) + \frac{D_0}{k_B T}\nabla^2\Bigg[k_B T \ln\left(\frac{c}{1-c}\right) - \epsilon_0 c - \xi_0^2\nabla^2 c + \sigma a^2[\varepsilon_{xx}(\mathbf{r}) + \varepsilon_{yy}(\mathbf{r})] + \sigma^2 a^4 \int_S d\mathbf{r}'\nabla_\alpha G_{\alpha\beta}(\mathbf{r}-r')\nabla'_\beta c(\mathbf{r}')\Bigg], \tag{22}$$

where $c_0 = \alpha/(\alpha+\beta)$ and $\tau^{-1} = \alpha+\beta$. The concentration c is in units of atom/atom. The introduction of the constant a^2, where a is the lattice constant, is for consistency of units.

III. NUMERICAL SOLUTION PROCEDURE

Because of the convolutional form of the integral in Eq. (21), a convenient way to solve the nonlinear partial differential-integral equation (28) is the Fourier spectral method. Let us denote the wave vector as $\mathbf{q}$, its amplitude as q, and the concentration in the transformed domain as c_q; then, by taking the Fourier transform (FT) of Eq. (22), we get

$$\partial_t c_\mathbf{q} = \frac{1}{\tau}(c_{0\mathbf{q}} - c_\mathbf{q}) - \frac{D_0}{k_B T}q^2\Bigg[\sigma a^2 \mathrm{Tr}(\varepsilon)_\mathbf{q} + k_B T\left\{\ln\left(\frac{c}{1-c}\right)\right\}_\mathbf{q} - [\epsilon_0 + \xi_0^2 q^2 + \sigma^2 a^4 q_\alpha q_\beta G_{\alpha\beta}(\mathbf{q})]c_\mathbf{q}\Bigg], \tag{23}$$

where $G_{\alpha\beta}(\mathbf{q})$ is the surface Green's function in Fourier space, which is evaluated by the analytical solution of general Green's functions on anisotropic substrates with cubic symmetry.[28] It is noted that the numerical technique relies on the application of periodic boundary conditions. We use a Galerkin approach to solve Eq. (23) in transformed space. Moreover, a pseudospectral technique is applied to nonlinear terms in the equation and an online split-radix fast FFT package written in FORTRAN code is adopted to implement the transformations.[29]

In order to have an efficient and accurate solution of the above ordinary differential equation, we adopt a semi-implicit second-order Adams-Bashforth backward differentiation function (AB-BDF) method, which is a stable time marching scheme.[30] The second-order BDF-AB scheme of Eq. (23) is given by

$$\left[3 + 2\Delta t\left(\frac{1}{\tau} + \epsilon_0 + \xi_0^2 q^2 + \sigma^2 a^4 q_\alpha q_\beta G_{\alpha\beta}(\mathbf{q})\right)\right]c_\mathbf{q}^{n+1} = 4c_\mathbf{q}^n - c_\mathbf{q}^{n-1} + 2\Delta t D_0 q^2\Bigg[2\left\{\ln\left(\frac{c^n}{1-c^n}\right)\right\}_\mathbf{q} - \left\{\ln\left(\frac{c^{n-1}}{1-c^{n-1}}\right)\right\}_\mathbf{q}\Bigg] + 2\Delta t\left[\frac{1}{\tau}c_{0\mathbf{q}} - \frac{D_0}{k_B T}q^2\sigma a^2 \mathrm{Tr}(\varepsilon)_\mathbf{q}\right]. \tag{24}$$

And the corresponding first-order scheme is expressed as

$$\left[1 + \Delta t\left(\frac{1}{\tau} + \epsilon_0 + \xi_0^2 q^2 + \sigma^2 a^4 q_\alpha q_\beta G_{\alpha\beta}(\mathbf{q})\right)\right]c_\mathbf{q}^{n+1} = c_\mathbf{q}^n + \Delta t D_0 q^2\left\{\ln\left(\frac{c^n}{1-c^n}\right)\right\}_\mathbf{q} + \Delta t\left[\frac{1}{\tau}c_{0\mathbf{q}} - \frac{D_0}{k_B T}q^2\sigma a^2 \mathrm{Tr}(\varepsilon)_\mathbf{q}\right]. \tag{25}$$

It should be emphasized that by solving the governing equations numerically, we consider the full logarithmic term instead of taking the expansion of the logarithm around the critical point by which it is in principle only valid close to the critical point. It will guarantee the validation of our simulation even far from it.

IV. RESULTS AND COMPARISON WITH EXPERIMENTS

A. Effects of external fields

A promising technique to manufacture nanostructures with uniform size and spatial distribution is to exploit the interplay between "natural" self-organization effects and "directed" self-organization due to applied fields. Practical sources of periodic external fields include applied electromagnetic fields over the substrate surface, buried periodic inclusions, and buried interfacial dislocation arrays, etc. An interesting experimental fact is that, in reality, uniform patterns can be formed with a fairly weak external field. Thus, the presence of a periodic external field acts to provide some preference for specific unstable modes, which appear to dominate all other nonpreferred unstable modes. For example, we can make an order-of-magnitude estimation of the strain field of buried interfacial dislocations as $\nu b/h$, where ν is Poission's ratio, b is Burgers' vector, and h is the thickness of the substrate layer to the surface. In recent experiments of Ge self-assembled quantum dots on the partially relaxed SiGe buffer layers,[17,18] the substrate thickness is about 80 nm and the length of Burgers' vector is ~0.2 nm. Thus the strain field is only on the order of 10^{-3}. If the intrinsic surface stress is assumed to be 1 eV per atom, according to Eq. (19), the interaction energy per atom is on the order of 10^{-3} eV ~ 10 K, which is two orders of magnitude lower than nearest-neighbor interaction (~10^3 K). Despite the weakness of this elastic field, Kim *et al.*[17,31] experimentally observed Ge quantum dots to nucleate along dislocation lines. At the same time, a denuded zone is formed on the other side of buried dislocations. We present here the results of numerical simulations that correspond to the experimental conditions of Kim *et al.*[17]

TABLE I. Model parameters for Ge adatoms on a $Si_{0.75}Ge_{0.25}$ substrate.

Notation	Parameter	Value	Units	Ref.
a	Lattice constant	0.566	nm	33
b_x	x's component of Burgers' vector	−0.193	nm	Estimated Ref. 33
b_z	z's component of Burgers' vector	−0.273	nm	Estimated Ref. 33
α	Adsorption rate	1.67×10^{-5}	$cm^2\ s^{-1}$	Estimated from Ref. 17
β	Desorption rate	1.67×10^{-6}	$cm^2\ s^{-1}$	Estimated from Ref. 17
D_s	Surface diffusion coefficient	2.57×10^{-7}	$cm^2\ s^{-1}$	31
σ	Intrinsic surface stress	1.6×10^{3}	erg/cm^2	14
c_{11}	Elastic constant	15.79×10^{11}	erg/cm^2	32
c_{12}	Elastic constant	6×10^{11}	erg/cm^2	32
c_{44}	Elastic constant	7.65×10^{11}	erg/cm^2	32

Specifically, we consider Ge atoms deposited on a $Si_{0.75}Ge_{0.25}$ substrate (see Table I). The Ge lattice constant a is 0.566 nm at room temperature. We take the pair potential ϵ_0 as about 0.3 eV. The adsorption α and evaporation rates β are assumed to be 1.67×10^{-5} $cm^2\ s^{-1}$ and 1.67×10^{-6} $cm^2\ s^{-1}$, respectively. The surface diffusion of Ge adatoms is strongly dependent on the temperature T and the coverage c. For simplicity, we assume that the surface diffusion coefficient D_s is constant and $D_s=D_0=2.57\times10^{-7}$ $cm^2\ s^{-1}$ (Ref. 31).

For calculations related with elastic interactions, we use the intrinsic surface stress σ as 100 meV $Å^{-2}$ for Ge(001), which is assumed to be equal to the Si(001) 2×1 surface by an order-of-magnitude estimation.[14] The elastic stiffness coefficients are $c_{11}=15.79\times10^{11}$ erg/cm^3, $c_{12}=6\times10^{11}$ erg/cm^3, and $c_{44}=7.65\times10^{11}$ erg/cm^3 (Ref. 32). The edge components of Burgers' vector of an interfacial dislocation in partially relaxed SiGe buffer layer are estimated directly by the equivalent lattice constants as $b_x\approx-1.93$ Å and $b_z\approx-2.73$ Å in which the negative sign means the extra half plane is downwards to infinity.

It should be noted that the numerical values of the above parameters have important effects on the chemical potentials in the system. It is thus expected that various parametric combinations can lead to different self-organization patterns. For example, different values of the lattice constant will possibly change the clustering behavior by imposing a different mismatch strain between adatoms and substrate atoms. In Sec. IV B, we develop an explicit expression [Eq. (30)], which allows studies of the effects of various parameter combinations by performing linear stability analysis.

Consider now one method to impose a periodic surface strain field by a network of interfacial dislocation between a thin film and a very thick substrate. Such an interfacial dislocation network can be experimentally obtained by bonding of the thin film to the thick substrate. The solution of the elasticity problem with the dislocation array can be formally obtained using 2D Fourier transforms in isotropic or anisotropic single layers[34] or multilayer systems.[35] However, we develop a simpler solution based on a single infinite straight dislocation in a homogeneous isotropic half space (Fig. 1). Using the complex variable representation method,[36] we represent the strain field with a simple equation

$$\varepsilon_{xx}=\frac{2}{\pi}\frac{(c_{11}-c_{12})}{(c_{11}+c_{12})}\frac{(b_x x+b_z h)xh}{(x^2+h^2)^2}, \tag{26}$$

where x is the horizontal distance along the surface measured from the dislocation, which is situated a distance h below the surface, as shown in Fig. 1. We may notice that the position of the maximum compressive strain is at the intersection of the extension of the extra half plane and the surface. It can be shown that if the extra half plane is in the upper buffer layer, the maximum compressive region will be the intersection of the slip plane and the surface. It is also found that the strain field decays significantly at distances greater than 1 μm from the dislocation. In the experiment of Kim *et al.*,[17] the distance between dislocations is about 9 μm. Thus, it is reasonable to ignore the interaction between dislocations and adopt the single dislocation solution (26) in the numerical periodic boundary condition. It should be noted that from Walgraef's results[11] the characteristic length of self-organized patterns without external perturbations is only on the order of 10 nm. For convenience, we will focus on the average coverage c_0 below the critical coverage in which the so-called 0 hexagons of dot patterns are selected.[37] We choose c_0

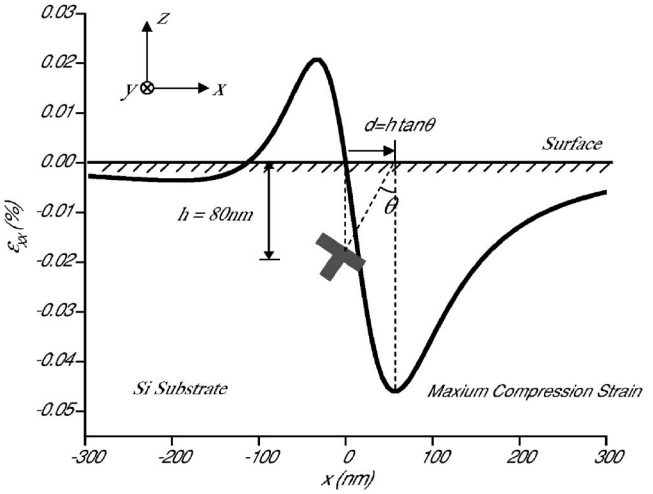

FIG. 1. Surface strain field of an interfacial dislocation buried at 80 nm underneath the Si surface, calculated by complex variable methods.

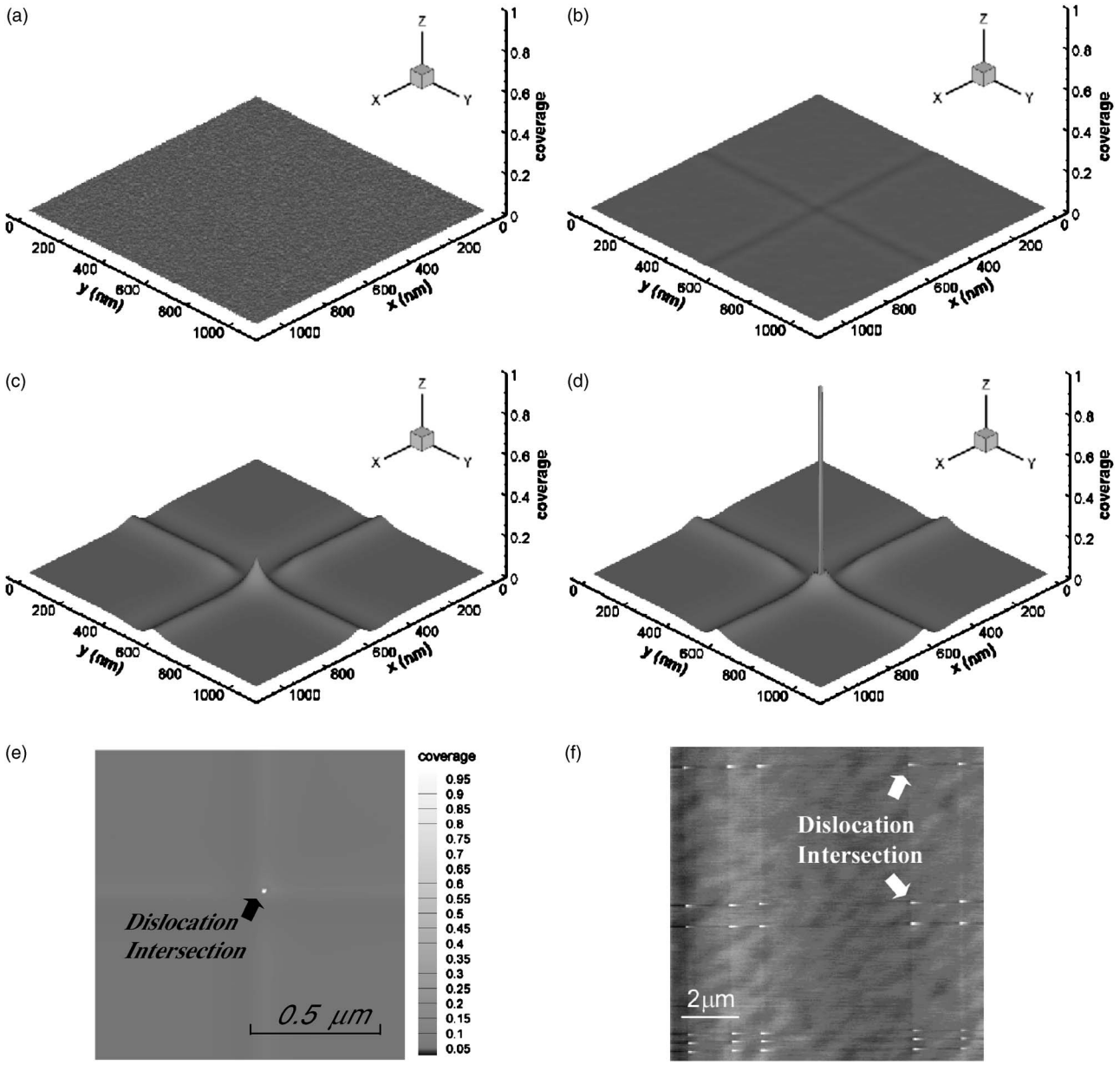

FIG. 2. Evolution of surface islands, starting with a small perturbation around $c_0=0.025$. The strain field is provided by two buried dislocations at a depth of 80 nm underneath the surface. (a), (b), (c), (d) 3D views of simulation results at 0 μs, 1.1 μs, 6.0 μs, and 9.3 μs, respectively. (e) The equilibrium state in a 2D view at 9.3 μs. (f) An optical micrograph of Kim *et al.* at a coverage of 4.0 Å (Ref. 17).

$=0.01-0.15$. In the experiments of Kim *et al.*,[17,31] Ge adatoms are deposited with Ge coverage ranging from 3 Å to 12 Å and then quenched to room temperature. Since the above formulation is for monolayer cluster formation and the Ge wetting-layer thickness is approximately 3 ML $\approx$4.2 Å,[38] the dynamic process in our model should be understood to represent the nucleation stage after a perfect wetting layer is formed. In the following results, a 1-μm^2 surface is divided into 256×256 grid points, which results in at least 2 points in the intrinsic characteristic length of the self-organized pattern.

All of our simulations begin with a small perturbation around c_0 at constant room temperature. Figures 2, 3, and 4 show the kinetic evolution processes for $c_0=0.025$, $c_0=0.05$, and $c_0=0.15$, respectively. It is observed that during the first 0.1 μs, a pattern quickly emerges with the intrinsic length scale of a self-organized structure. At the same time, the global distribution is adjusted by the external strain field. As the evolution process continues, for $c_0=0.025$, the dots nucleate exclusively at the intersections of dislocation lines. However, for $c_0=0.05$ all dots except those along dislocations are completely wiped out by the applied strain field at about 1 μs. Then a clear distribution of dots is formed along dislocation lines. For the case of $c_0=0.15$, the dots keep on growing by association. The pattern becomes especially denser in the region with the maximum compressive field along the dislocations until reaching equilibrium. A denuded zone, with a length scale of the order of 0.1 μm, is formed in the maximum compression region on the other side of dislocations. These results clearly show the three stages of nucle-

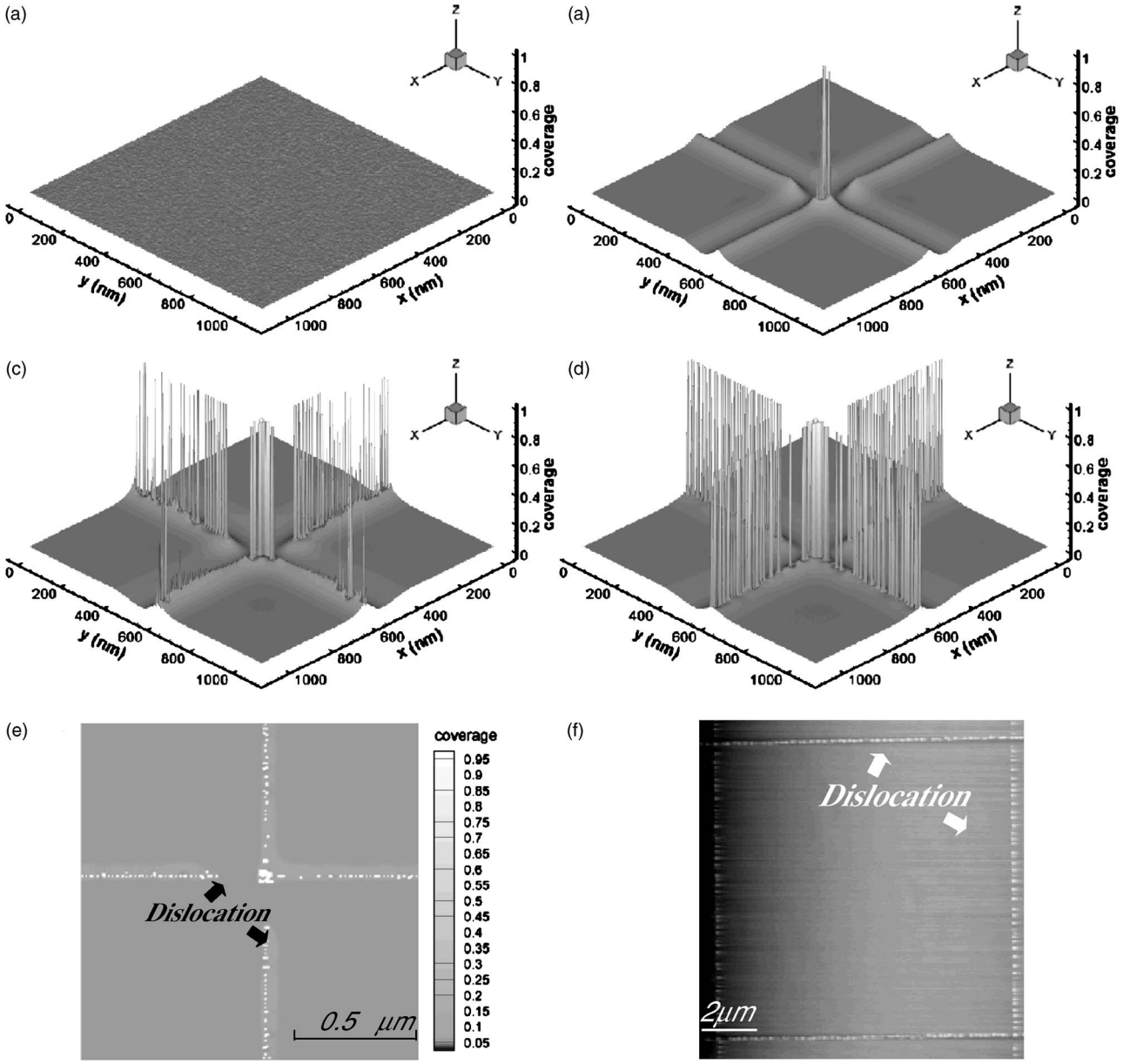

FIG. 3. Evolution of surface islands, starting with a small perturbation around $c_0=0.05$. The strain field is provided by two buried dislocations at a depth of 80 nm underneath the surface. (a), (b), (c), (d) 3D views of simulation results at 0 μs, 8.25 μs, 10.45 μs, and 15.95 μs, respectively. (e) The equilibrium state in a 2D view at 18 μs. (f) An optical micrograph of Kim *et al.* at the coverage of 4.5 Å (Ref. 17).

ation, which is consistent with experimental atomic force microscope (AFM) images.[17] It can be noticed that both our simulation results and the experimental results show an asymmetric distribution of quantum dots and denuded zones on the two sides of dislocations, which is induced by the asymmetry of external fields as shown in Fig. 1.

In order to quantitatively describe different distributions of surface atomic clusters, we construct a quantity that is analogous to the mass moment of inertia:

$$I_{xx} = \int d^2r(x - x_c)^2 c(\mathbf{r}), \tag{27}$$

where x_c is the x component of the center of mass and is defined as

$$x_c = \frac{\int d^2rxc(\mathbf{r})}{\int d^2rc(\mathbf{r})}.$$

We carry out calculations for one buried dislocation along the y direction and compare the results with different average coverage c_0. In this case, the smaller the value I_{xx}, the larger the influence of the external field. It is shown in Fig. 5 that when c_0 is very small—say, 0.01—adatom clusters are uniformly distributed and that the distribution is shaped by the external field. The integral in Eq. (27) is the surface integral, and the limits of it are the area of the simulation surface. I_0 in

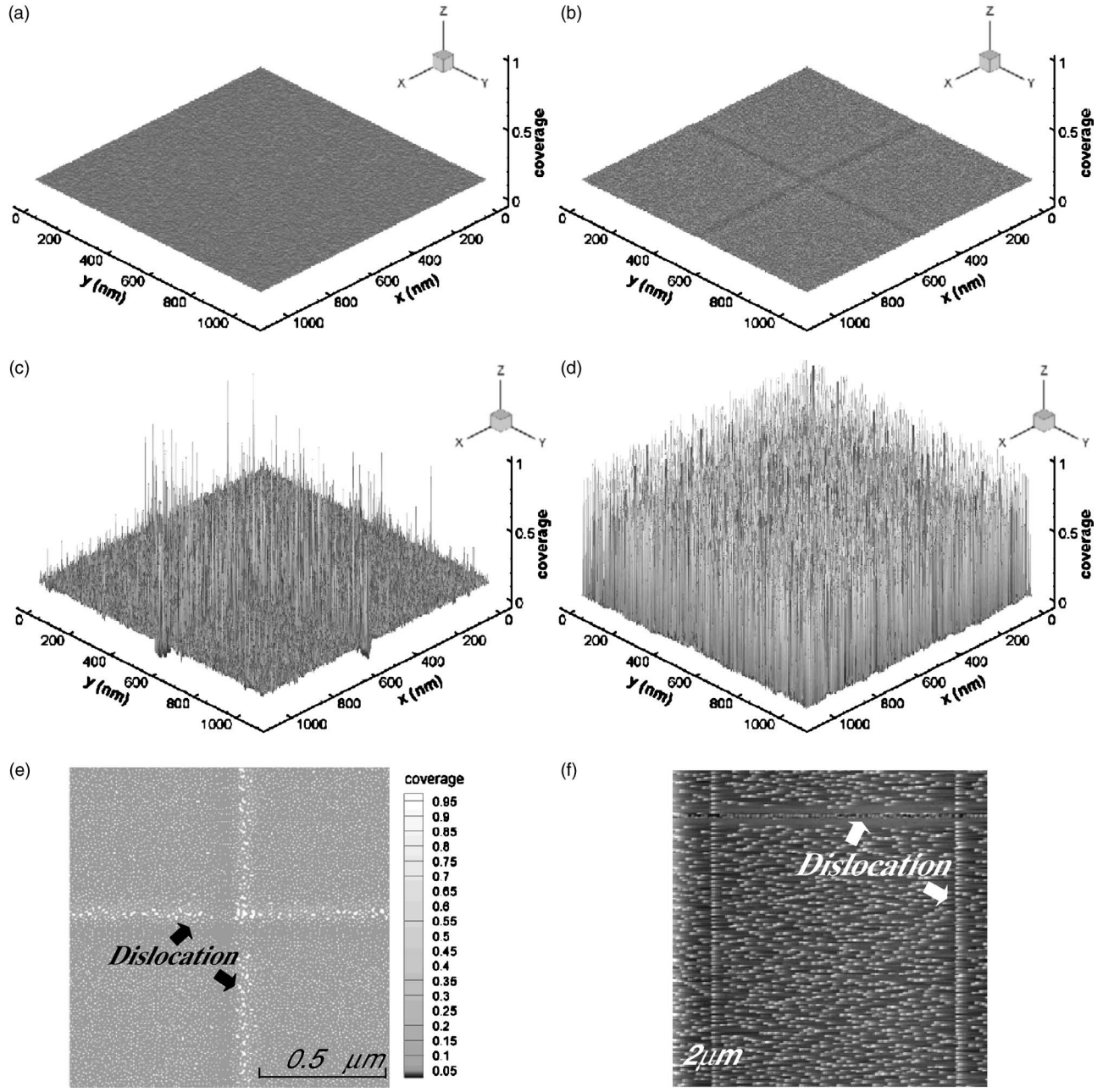

FIG. 4. Evolution of surface islands, starting with a small perturbation around c_0=0.15. The strain field is provided by two buried dislocations at a depth of 80 nm underneath the surface. (a), (b), (c), (d) 3D views of simulation results at 0 μs, 0.22 μs, 0.55 μs, and 1.1 μs, respectively. (e) The equilibrium state in a 2D view at 10.45 μs. (f) An optical micrograph of Kim *et al.* at the coverage of 6.0 Å (Ref. 17).

Fig. 5 is a constant and is defined as the uniform distribution of atoms. In this case, the instability does not take place and dots do not form. When c_0 increases to 0.05, an instability takes place and there is a strong influence of the external strain field at a time of about 10 μs. All stripes emerge into one sharp soliton profile. In this case, the directed self-organized pattern becomes dominant. As c_0 is set to larger than 0.05—say, equal to 0.15—the natural self-organized pattern interacts with the directed self-organized pattern. It can be seen that there is a high density of atomic clusters on the maximum compression side along the dislocation line and a sparse distribution on the other side. The interaction between the external field and the emerging patterns results from strong coupling between the wave vectors provided by the external field periodicity and the corresponding unstable wave vectors of the self-organized pattern.

B. Effects of cluster-cluster interactions

We will consider here the effects of cluster-cluster (CC) interactions on the natural self-organization behavior of surface clusters. Thus, we assume that there is no applied external field ($\varepsilon_{\alpha\alpha}$=0) or that the external field is uniform ($\nabla^2\varepsilon_{\alpha\alpha}$=0). More generally, Eq. (22) can be written in dimensionless form as

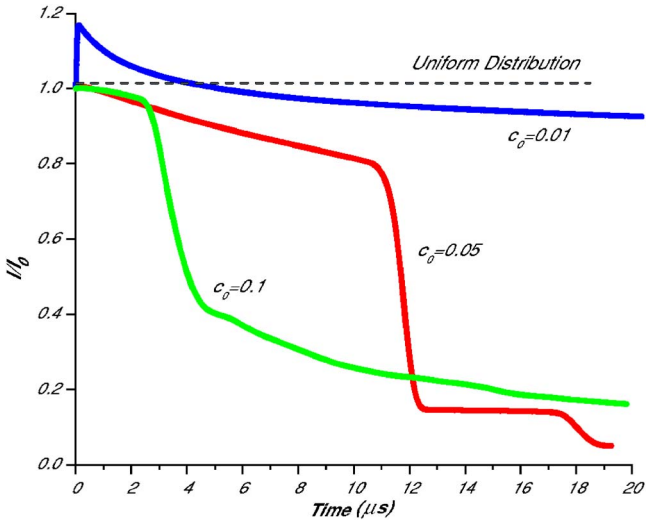

FIG. 5. (Color online) The relative mass moment of inertia as a function of time for a buried dislocation at 80 nm depth from the surface for different initial concentrations.

$$\tau\partial_t\hat{c} = (\hat{c}_0 - \hat{c}) + \hat{D}\nabla^2\left[-\frac{T_c}{T}\hat{c} + \frac{1}{4}\ln\left(\frac{1+2\hat{c}}{1-2\hat{c}}\right) - \frac{\xi_0^2}{4k_BT}\nabla^2\hat{c} + \frac{\sigma^2 a^4}{4k_BT}\int d\mathbf{r}'\nabla_i G_{ij}(\mathbf{r}-r')\nabla_j'\hat{c}(\mathbf{r}')\right], \tag{28}$$

where $\hat{c}=c-\frac{1}{2}$, $\hat{D}=4\tau D_0$, and $T_c=\epsilon_0/4k_B$. Considering small perturbations ς about the steady state $\hat{c}_0$ ($\varsigma=\hat{c}-\hat{c}_0$), we can expand the mixing entropy term in a first-order Taylor series and use the relation

$$\int d\mathbf{r}'\nabla_i G_{ij}(\mathbf{r}-r')\nabla_j'\hat{c}(\mathbf{r}') \to q_i q_j\{G_{ij}\}_{\mathbf{q}}c_{\mathbf{q}}$$

to rewrite Eq. (28) in Fourier space as

$$\tau\partial_t\varsigma(\mathbf{q}) = -\left[1 + q^2\frac{\hat{D}^*T_c^*}{T}\left(\frac{T}{T_c^*} - 1 + A^2q^2 - B^2q_iq_jG_{ij}(\mathbf{q})\right)\right]\varsigma(\mathbf{q}), \tag{29}$$

where $T_c^*=T_c(1-4\hat{c}_0^2)$, $D^*=\hat{D}/(1-4\hat{c}_0^2)$, $A^2=\xi_0^2/4k_BT_c$, and $B^2=\sigma^2/4k_BT_c$. The marginal stability curve is given by

$$T^* = q^2D^*T_c^*\frac{1 - A^2q^2 + B^2q_iq_jG_{ij}(\mathbf{q})}{1+q^2D^*}. \tag{30}$$

Here, the critical temperature T^* is the temperature that determines the transition from stable (uniform) solution to an unstable (patterned) solution. It can be seen from Eq. (30) that the critical temperature is determined by a set of *reduced* parameters, which include D^*, T_c^*, A, B, and all components of $G_{ij}(\mathbf{q})$. The original parameters—e.g., lattice constants, desorption and adsorption rates, pair potentials—are combined now in the new reduced set. In other words, various combinations of these parameters in the numerical simulation will give completely different "phases" of the system, as shown in Fig. 6. Our numerical simulations show consistency with theoretical predictions given by Eq. (30).

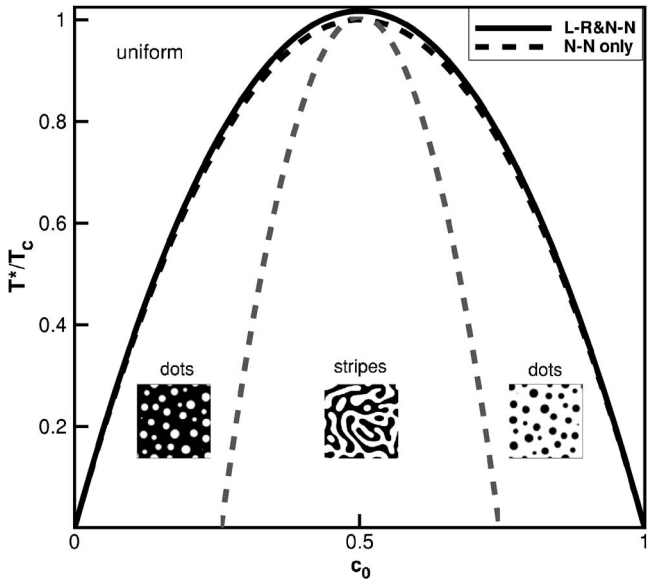

FIG. 6. "Phase diagram" for monolayer surface patterns, showing the small influence of long-range interactions. The dot-stripe separation curve is adopted from Walgraef's work of weak nonlinear stability analysis (Ref. 11).

After numerically calculating the maximum point of T in the above equation, we obtain a relationship between the critical temperature T^* and the control parameter c_0. In Fig. 6, we compare the two cases with NN interactions only and with both CC and NN interactions, respectively. The black dashed curve is obtained from Eq. (30) with $G_{ij}=0$. The gray dashed curve can only be obtained from the weak nonlinear stability analysis which we adopted the whole calculation from Walgraef's work.[11] It is shown that cluster-cluster interactions have a q^3 destabilizing effect and that the maximum change at $c_0=0.5$ is about 1.75% T_c. Thus, the distablizing effect of CC interactions is small.

In addition to their destabilizing effects, CC interactions have more important effects on patterning. In Fig. 7, we compare the results of simulation for a surface area of 100×100 nm^2 without external fields at an average coverage of $c_0=0.5$. The system should develop a stripe pattern,[11] similar to the simulations of Proville.[10] It is noted that when we include CC interactions, stripes becomes sharper and are ori-

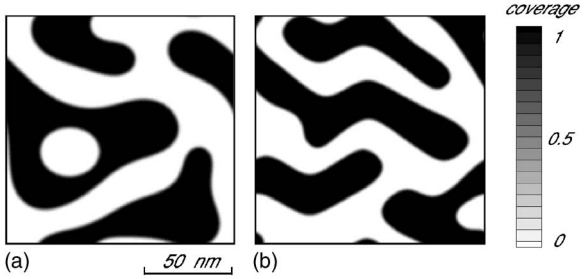

FIG. 7. The equilibrium results at the time of 10 μs with the average coverage of $c_0=0.5$ where the gray scale is proportional to coverage. (a) NN interactions only. (b) NN and CC interactions.

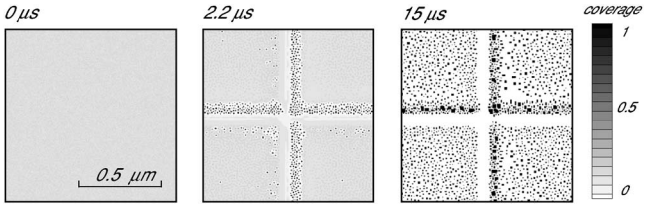

FIG. 8. Cluster evolution with NN interaction only, for the case of two crossing interfacial dislocations buried at 80 nm below the surface, where the gray scale is proportional to the coverage.

ented along the elasticity anisotropy axes of the material. In Fig. 8, the simulation is carried over a large system ($1 \times 1\ \mu m^2$) without a dislocation network underneath the surface. It is seen by comparing with Fig. 7, that CC interactions increase the density of dots, but the average size of dots becomes smaller. Also the denuded zone is much sharper if no CC interactions are included.

V. CONCLUSIONS

In the present paper, we set up a phase-field model to describe monolayer cluster evolution on the surface. We include in this model the effects of interactions mediated by the substrate, expressing these interactions as gradients of intrinsic surface stresses. The direct interaction between clusters and applied non uniform strain fields is included in the model without the dependence on coverage, while cluster-cluster interaction effects are accounted for as a function of concentration. Such cluster-cluster interactions are inherently long range, and they exist because of force transmission through the substrate.

The present study is focused on two main effects. First, the effects of long-range CC interactions are explored, and second, we determine the influence of an externally applied strain field on the characteristics of surface patterns. It is found that the effects of long-range CC interactions are rather weak and that they change the stability ranges of emerging patterns by only a few percent. On the other hand, we found that CC interactions tend to enhance the stability of striped patterns at a fine scale.

The main question in the present investigation is the manner by which an external strain field influences emerging patterns. To quantify such effects, we studied the case of a periodic surface strain field obtained by an interfacial dislocation array. It is surprising to find that although the imposed strain field is weak, providing an energy contribution of $\sim 10^{-3}$ eV, it profoundly affects pattern selection and stability. It is found that the spatial and size distribution of adatom clusters is a result of an interplay between "natural" self-organization and directed self-organization provided by external fields, even for a strain field as weak as 10^{-3}. In the specific case of buried dislocations, for an average coverage greater than 0.15 monolayer, clusters tend to agglomerate at the compressive side of dislocations. For an even lower coverage not below the critical coverage, such as 0.01, we could obtain dots distributed uniformly along the dislocation lines.

Since we only investigate the early stages of nucleation with very low coverage, we reasonably ignored the effects of the mass redistribution between the wetting layer and quantum dots. It should be emphasized that our phase-field model is based on a monolayer structure of clusters. For the interfacial dislocation case in the SiGe system in comparison with experimental results,[17] our model should be understood as applicable for cluster evolution after the wetting layer is formed. In addition, even the dots observed in experiments are multilayer structures. In order to develop a 3D island formation model, a multilayer deposition process can be added to the present model. However, the qualitative agreements between the monolayer model and the experiments indicate that island nucleation is mainly determined by monolayer stages and the 3D construction of islands will not have a dramatic effect on the selected patten of quantum dots or on its stability..

*Electronic address: huqy@ucla.edu
†Electronic address: ghoniem@ucla.edu

[1] G. H. Gilmer and P. Bennema, J. Appl. Phys. **43**, 1347 (1971).
[2] H. Huang, G. H. Gilmer, and T. Diaz de la Rubia, J. Appl. Phys. **84**, 3636 (1998).
[3] Q. Hu and N. M. Ghoniem, J. Comput. Theor. Nanosci. **3**, 696 (2006).
[4] T. R. Mattsson and H. Metiu, J. Chem. Phys. **113**, 10323 (2000).
[5] A. G. Khachaturyan, *Theory of Structural Transformations in Solids* (Wiley, New York, 1983).
[6] C. A. Laberge, P. Fratzl, and J. L. Lebowitz, Phys. Rev. Lett. **75**, 4448 (1995).
[7] Y. Wang, L.-Q. Chen, and A. G. Khachaturyan, Acta Metall. Mater. **41**, 279 (1993).
[8] Z. Suo and W. Lu, J. Nanopart. Res. **2**, 333 (2000).
[9] W. Lu and Z. Suo, J. Mech. Phys. Solids **49**, 1937 (2001).
[10] L. Proville, Phys. Rev. B **64**, 165406 (2001).
[11] D. Walgraef, Philos. Mag. **83**, 3829 (2003).
[12] B. J. Spencer, P. W. Voorhees, and S. H. Davis, Phys. Rev. Lett. **67**, 3696 (1991).
[13] P. Berger, P. Kohlert, K. Kassner, and C. Misbah, Phys. Rev. Lett. **90**, 176103 (2003).
[14] V. A. Shchukin, A. I. Borovkov, N. N. Ledentsov, and D. Bimberg, Phys. Rev. B **51**, 10104 (1995).
[15] V. I. Marchenko and A. Y. Parshin, Sov. Phys. JETP **52**, 129 (1980).
[16] O. L. Alerhand, D. Vanderbilt, R. D. Meade, and J. D. Joannopoulos, Phys. Rev. Lett. **61**, 1973 (1988).
[17] H. J. Kim, Z. M. Zhao, and Y. H. Xie, Phys. Rev. B **68**, 205312 (2003).
[18] H. J. Kim, Z. M. Zhao, J. Liu, V. Ozolins, J. Y. Chang, and Y. H. Xie, J. Appl. Phys. **95**, 6065 (2004).
[19] G. Springholz, C. R. Phys. **6**, 89 (2005).
[20] N. M. Ghoniem, D. Walgraef, and S. J. Zinkle, J. Comput.-Aided

Mater. Des. **8**, 1 (2002).
[21] J. S. Langer, Ann. Phys. (N.Y.) **54**, 258 (1969).
[22] A. Roy, J. M. Rickman, J. D. Gunton, and K. R. Elder, Phys. Rev. E **57**, 2610 (1998).
[23] J. W. Cahn, J. Chem. Phys. **42**, 93 (1965).
[24] T. Wanner, Trans. Am. Math. Soc. **356**, 2251 (2004).
[25] D. Groot and P. Mazur, *Non-Equilibrium Thermodynamics* (Dover, New York, 1984).
[26] K. H. Lau and W. Kohn, Surf. Sci. **65**, 607 (1977).
[27] L. D. Landau and E. M. Lifshitz, *Fluid Mechanics* (Pergamon, New York, 1987).
[28] K. Portz and A. A. Maradudin, Phys. Rev. B **16**, 3535 (1977).
[29] T. Ooura, http://momonga.t.u-tokyo.ac.jp/ooura/fft.html.
[30] L. Q. Chen and J. Shen, Comput. Phys. Commun. **108**, 147 (1998).
[31] H. J. Kim, J. Y. Chang, and Y. H. Xie, J. Cryst. Growth **247**, 251 (2003).
[32] *Numerical Data and Functional Relationships in Science and Technology*, edited by K. Hellwege and O. Madelung (Springer, Berlin, 1982), vol. III.
[33] C. Kittel, *Introduction to Solid State Physics* (Wiley, New York, 1986).
[34] J. R. Willis, S. C. Jain, and R. Bullough, Philos. Mag. A **62**, 115 (1990).
[35] X. Han and N. M. Ghoniem, Philos. Mag. **85**, 1205 (2005).
[36] Z. Suo, Int. J. Solids Struct. **25**, 1133 (1989).
[37] D. Walgraef, *Spatio-Temporal Pattern Formation, With Examples from Physics, Chemistry, and Material Science* (Springer, Berlin, 1997).
[38] Y.-W. Mo, D. E. Savage, B. S. Swartzentruber, and M. G. Lagally, Phys. Rev. Lett. **65**, 1020 (1990).